applied sciences

MDPI

Article

Current Sensorless MPPT Control for PV Systems Based on Robust Observer

David Cortes-Vega, **Hussain Alazki *** and **Jose Luis Rullan-Lara**

Faculty of Engineering, Universidad Autonoma del Carmen, Ciudad del Carmen 24180, Campeche, Mexico; dcortesvega@gmail.com (D.C.-V.); jrullan@delfin.unacar.mx (J.L.R.-L.)
* Correspondence: khussinaz@yahoo.com

Abstract: Photovoltaic (PV) systems are among the most used alternatives for electrical power generation from renewable sources. To ensure that PV systems make the most of the available solar energy, maximum power point tracking (MPPT) schemes must be implemented, which usually require voltage and current sensors to track the PV power. This paper presents the design of a robust observer using the Attractive Ellipsoid Method to achieve a precise estimation of PV current under parametric uncertainty and output perturbations. The application of such an observer enables the PV generation system to operate in a current sensorless mode, which reduces the overall cost of the system and enhances its reliability. The convergence of the observer is guaranteed by solving an optimization problem which generates the optimal gains using Linear Matrix Inequalities (LMI). To prove the effectiveness of the proposed sensorless scheme, simulations are performed in Matlab under test profiles based on the EN50530 standard and parameter uncertainty conditions, obtaining an accurate estimation which is used for MPPT operation.

Keywords: PV system; current sensorless operation; boost converter; observer; maximum power point tracking

Citation: Cortes-Vega, D.; Alazki, H.; Rullan-Lara, J.L. Current Sensorless MPPT Control for PV Systems Based on Robust Observer. *Appl. Sci.* **2022**, *12*, 4360. https://doi.org/10.3390/app12094360

Academic Editors: Isabel Santiago Chiquero, Isabel María Moreno García and Rafael López Luque

Received: 8 April 2022
Accepted: 21 April 2022
Published: 26 April 2022

1. Introduction

The utilization of solar energy as an alternative for electrical energy generation has shown a great improvements in recent decades. This is motivated by a global interest in developing green energy sources with a lower environmental impact in contrast with the traditional schemes based on fossil fuels. Nowadays, due to technological development related to photovoltaic (PV) systems, the associated system costs lowered and the efficiency of panels and components increased. These developments have given rise to the generation of PV systems for a broad range of applications from low power domestic use to large generation sites for industrial usage.

In order to make the most from the available solar energy, a PV system requires maximum power point tracking (MPPT) techniques that allow the system to operate in optimal conditions, guaranteeing the extraction of maximum power at every instant. There are several MPPT techniques with different characteristics that range from the most common schemes as the Perturb and Observe (PO) algorithm [1], incremental conductance (INC) [2] or fractional open circuit voltage, to novel and more complex approaches as artificial neural networks [3], genetic algorithms [4], fuzzy logic [5], among others. However, nowadays the most commonly used MPPT schemes are still the first ones due to its ease of implementation and capability to operate without knowledge about PV system characteristics requiring only voltage and current measurements. Hence, the system requires voltage and current sensors to perform MPPT operation which increases the overall system cost and reduces its reliability by possible sensor faults. The voltage of the PV array can be measured in a simple way using a potential divider arrangement for non-isolated measurement. On the other hand, the current measurement shows more difficulties, where Shunt resistors or Hall effect sensors are commonly used. The Shunt resistor based sensors obtain the current value in terms of voltage by means of voltage drops across them. Hence, a heat power dissipation exists across this type of sensor because of Joule's effect which affects the measurement, so it requires low tolerance, high precision and low temperature drift resistance [6,7]. Further, to perform the current measurement in a proper scale it is necessary to increase the value of shunt resistance which will also increase the heat dissipation. Moreover, when low values of PV arrangement current are measured the sensor provides an almost undetectable output which needs to be amplified increasing the number of components and overall system cost. On the other hand, Hall effect sensors use measurements of the magnetic field generated by the current of interest. Therefore, this type of current sensor is easily affected by external magnetic fields [8,9]. So, the precision of current measurements from Hall effect sensors is affected by the conductor and sensor position [10]. Conventional MPPT controllers using Hall Effect sensors, include additional circuitry, like signal conditioning buffers and amplifier circuits to filter out the high frequency components caused by the converter switching. However, this increases the cost and complexity of the PV system.

Thus, elimination of the current sensor can be a convenient option to provide some key benefits in PV systems as cost reduction, low maintenance and more reliability, particularly when working with systems using multi-level or cascaded topologies [11]. In the related literature one can find different current sensorless schemes that allows the system to dispense with the use of a current sensor. In [12], a current sensorless method is presented which is based on the estimation of the PV current by shorting the two terminals of the PV system. However, such technique will decrease the life of the components connected to the PV terminals and also the PV panel itself. A sensorless MPPT scheme based on Internet of Things is proposed in [13] using public domain solar irradiation data from Internet. Nevertheless, this approach efficiency is obviously dependent on the accuracy of the local website data about the PV system location. Further, because of its inaccurate forecasting of temperatures, it may lead to operate at a point far from the maximum power point.

The unscented Kalman filter and Extended Kalman filter are implemented to estimate the inductor current in a boost converter based PV system obtaining an accurate estimation [14,15]. However, both techniques are computationally intensive due to the use of non-linear transformations and linearization procedures [16,17]. A current sensorless method based on finite control set model predictive control (MPC) with auto-tuning is developed in [18]. MPC is a powerful technique, but its applicability is limited because of its complexity of implementation, mainly in small scale PV systems. The sliding modes technique has been used to design robust observers to estimate voltages and currents in PV systems with good results against different perturbations and operating conditions [19,20]. However, the main drawback of this technique is the chattering problem which reduces the life of components. The high gain observers are another alternative used for robust current estimation in PV systems. As shown in [21] a high gain observer is designed to estimate voltage and current in a pumping system supplied by a PV generator. Although a precise estimation is performed, the disadvantages of this approach are the sensitivity to measurement noise and the peaking phenomenon [22]. In [23], a Luenberger observer is proposed to estimate the current and this estimation is used in a PO scheme for MPPT, the proposal is effective and easy to implement but lacks robustness since there is no consideration about system uncertainties or external perturbations at the output. Due to its effectiveness and ease of implementation, a Luenberger observer is a good alternative for current estimation but requires a robust design to improve its efficiency under disturbance scenarios.

The Attractive Ellipsoid Method (AEM) is a tool used for synthesis of robust feedback controllers with respect to a wide class of uncertainties contained in the system's model. This methodology guarantees system stability by finding appropriate controller gains obtained through the definition and solution of an optimization problem in terms of Linear Matrix Inequalities (LMI) or Bilinear Matrix Inequalities (BMI) [24]. System motion stabilization to zero is not always possible when external disturbances, uncertainties or nonlinearities are present in a system, in such cases only boundedness of trajectories within some compact set is guaranteed. This boundedness is commonly obtained through invariant sets. Ellipsoidal sets possess such invariant condition and can be obtained using the invariant ellipsoid method, called attractive ellipsoid method if this condition is ensured for any initial conditions [24]. These ellipsoidal sets can be designed to obtain certain minimal properties related to ellipsoid size, volume, among others, which may be used for design of robust observers/controllers for several applications [25,26]. The optimization problems based on LMI/BMI derived from application of AEM can be solved using semi-definite programming or specialized BMI solvers.

Therefore, this paper proposes the design of a robust Luenberger state observer based on AEM which allows a current sensorless operation that improves the reliability at the same time that reduces the overall system cost. Such proposed robust observer guarantees a low estimation error that ensures the proper application of MPPT algorithms which requires PV current measurement. Furthermore, this observer is robust against output disturbances and parameter uncertainties on the PV system components which contributes to obtain a more accurate estimation under such conditions. In order to demonstrate the effectiveness of the proposed robust observer a simulation of an INC-MPPT sensorless scheme is performed in Simulink under the european standard EN-5060.

The remainder of this paper is organized as follows: Section 2 presents the system model considering a boost converter based PV system. Section 3 focuses on the problem formulation introducing some mathematical concepts required to apply AEM, while Section 4 is devoted to the robust observer design process and the introduction of Incremental Conductance MPPT scheme. Section 5 presents numerical simulation results to show the effectiveness of the proposed observer and the implementation of the sensorless scheme for MPPT operation under test profiles based on EN50530 standard. Finally, Section 6 states the main conclusions and some directions for future research.

2. System Modeling

The overall PV generation system is composed of a PV array, a DC-DC boost converter and a load, as illustrated in Figure 1. In order to design a robust observer based on AEM a quasi-Lipschitz model representation is required which states that the system is bounded in a particular way. Hence, this section details the mathematical model considered for boost converter and its quasi-Lipschitz representation.

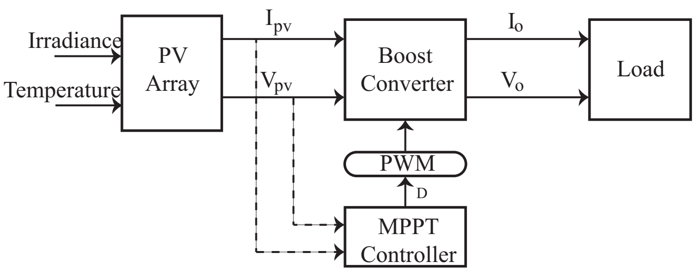

(a)

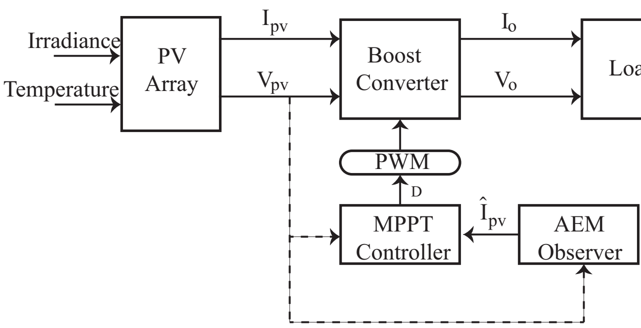

(b)

Figure 1. PV System's configurations. (**a**) Conventional PV system with voltage and current sensors; (**b**) Proposed PV system with current estimation.

Boost Converter Model

Power converters, specifically DC-DC type, are widely used in PV generation systems as an adaptation stage between PV panels and the load being supplied [27,28]. The main objective of such converters is to adjust the PV array output voltage in order to maximize the power generation. One of the most used topologies for PV systems is the boost configuration which is shown in Figure 2, where V_{pv} is the PV array voltage, V_s is the output voltage and i_L which is the inductor current is assumed to be equal to I_{pv}. The remaining components C, L and R are the output capacitor, inductor and converter load, respectively.

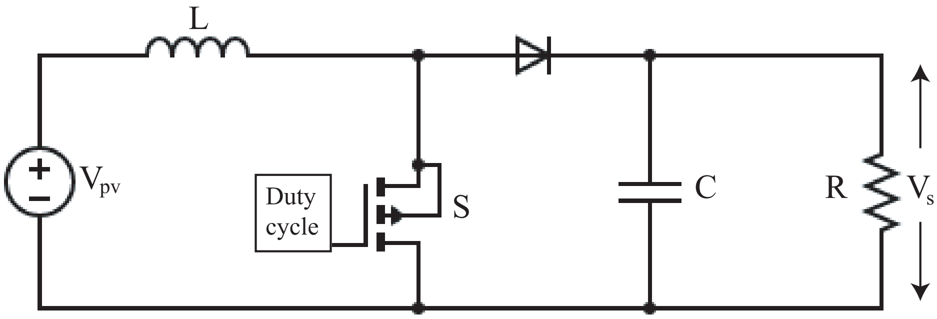

Figure 2. Boost converter topology.

Depending on the switch (S) state and considering only the continuous conduction mode, the boost converter can be represented by means of state equations by the following cases.

Case 1: Switch is in OFF state, the load is supplied by energy stored in the inductor, applying Kirchhoff's laws, voltage and current dynamics can be described as

$$\frac{d}{dt}\begin{bmatrix} I_L \\ V_s \end{bmatrix} = \underbrace{\begin{bmatrix} 0 & -\frac{1}{L} \\ \frac{1}{C} & -\frac{1}{RC} \end{bmatrix}}_{A_{OFF}} \begin{bmatrix} I_L \\ V_s \end{bmatrix} + \underbrace{\begin{bmatrix} \frac{V_{pv}}{L} \\ 0 \end{bmatrix}}_{b_{OFF}} \tag{1}$$

Case 2: Switch is in ON state, the inductor is charged by the input voltage V_{pv} and the load is disconnected, applying Kirchhoff's laws, voltage and current dynamics can be described as

$$\frac{d}{dt}\begin{bmatrix} I_L \\ V_s \end{bmatrix} = \underbrace{\begin{bmatrix} 0 & 0 \\ 0 & -\frac{1}{RC} \end{bmatrix}}_{A_{ON}} \begin{bmatrix} I_L \\ V_s \end{bmatrix} + \underbrace{\begin{bmatrix} \frac{V_{pv}}{L} \\ 0 \end{bmatrix}}_{b_{ON}} \tag{2}$$

From the above cases, defining $x_a = [I_L, V_s]^T$ the dynamic behavior during ON-OFF periods can be expressed as follows

$$\dot{x}_a = Ax_a + b \tag{3}$$

Considering that $\mu = 1$ when the switch is ON and $\mu = 0$ when switch is OFF, Equation (3) can be expressed as [29,30]

$$\dot{x}_a = A_{OFF}x_a + b_{OFF} + (A_{ON} - A_{OFF})x_a\mu + (b_{ON} - b_{OFF})\mu \tag{4}$$

In boost topology $b_{ON} = b_{OFF}$, which leads to

$$\dot{x}_a = A_{OFF}x_a + b_{OFF} + (A_{ON} - A_{OFF})x_a\mu \tag{5}$$

Under the assumption that a high switching frequency is present the corresponding average state space model [31,32] for (1) and (2) is described by

$$\begin{aligned}\dot{x}_1 &= \frac{V_{pv}}{L} - \frac{x_2(1-u)}{L} \\ \dot{x}_2 &= \frac{x_1(1-u)}{C} - \frac{x_2}{RC}\end{aligned} \tag{6}$$

where $u \in [0\ 1]$ is the average value of converter's duty cycle and $x = [I_L, V_s]^T$ represents the average values of inductor current and converter output voltage.

The relation between boost converter output voltage (V_s) and the PV array voltage (V_{pv}) is described by

$$\frac{V_s}{V_{pv}} = \frac{1}{1-u} \tag{7}$$

3. Problem Formulation

A current sensorless PV system requires the capability to track the maximum power point at every instant with high precision even when model uncertainties arise. Such objective can be achieved using a robust estimation scheme which allows any current dependent MPPT technique to drive system towards MPP. To perform this estimation task in a fast and accurate form under model uncertainty conditions, a robust Luenberger observer based on AEM is proposed and INC algorithm is applied to generate the voltage references that move the system around the MPP.

3.1. Mathematical Preliminaries

This subsection introduces some important definitions and results required for the application of AEM.

Considering a general nonlinear system described as

$$\begin{aligned}\dot{x} &= f(x) \\ x(0) &= x_0 \in \mathbb{R}^n\end{aligned} \tag{8}$$

where $f : \mathbb{R}^n \times \mathbb{R}^m \mapsto \mathbb{R}^n$ is a suitable right hand side.

Definition 1. *A set $\mathcal{H}$ is said to be positively invariant for the system*

$$\dot{x} = f(x)$$

if $x(t) \in \mathcal{H}$ for every $x(0) \in \mathcal{H}$ and for all $t \geq 0$.

The class of systems which are suitable for the proposed robust observer design are a particular class of nonlinear systems known as quasi-Lipschitz dynamic models with bounded uncertainties. The formal definition of a quasi-Lipschitz function is presented as follows [24].

Definition 2. *A vector function $f : \mathbb{R}^n \to \mathbb{R}^k$ is said to be a quasi-Lipschitz function $\mathcal{Q}(A, \eta_0, \eta_1)$ if there is a matrix $A \in \mathbb{R}^{k\times n}$ and nonnegative constants η_0 and η_1, such that for every $x \in \mathbb{R}^n$, the following inequality holds:*

$$\|f(x) - Ax\|^2 \leq \eta_0 + \eta_1\|x\|^2. \tag{9}$$

Hence, system (6) can be represented as follows

$$\dot{x} = Ax + g(x)u + \phi \quad , \tag{10}$$

where $x \in \mathbb{R}^n$ is the state vector, $A \in \mathbb{R}^{n\times n}$ is the system matrix, $g(x) \in \mathbb{R}^{n\times m}$ is the control function, $u \in \mathbb{R}^m$ is the vector of control inputs, and $\phi = f(x) - Ax$, is an uncertain vector function assumed to satisfy quasi-Lipschitz condition, as stated in (9). To guarantee an appropriate design, the pair (A, C) must be determined such that the system is observable.

3.2. Bounded System Model Representation

In order to apply the AEM, the selected model needs to be described in a particular way satisfying the quasi-Lipschitz condition. This section focuses on the analysis of system model characteristics and its representation in such bounded form.

The PV system model is represented in the following form

$$\dot{x} = Ax + g(x)u + \phi \tag{11}$$

$$y = h(x) + w$$

where

$$A = \begin{bmatrix} 0 & -\frac{1}{L} \\ \frac{1}{C} & -\frac{1}{R_L C} \end{bmatrix}, \quad g(x) = \begin{bmatrix} \frac{b_2}{L} \\ \frac{-b_1}{C} \end{bmatrix}$$

$$\phi = \begin{bmatrix} \gamma_1 V_{pv} \\ -\gamma_2 + \gamma_3 \end{bmatrix}$$

$$\gamma_1 = \frac{\Delta L}{L(L + \Delta L)}, \quad \gamma_2 = \frac{\Delta C}{C(C + \Delta C)}$$

$$\gamma_3 = \frac{R\Delta C + C\Delta R + \Delta R \Delta C}{RC(RC + R\Delta C + C\Delta R + \Delta R \Delta C)}$$

and $\Delta(\cdot)$ represents a parametric uncertainty in the component.

The term ϕ is required to be bounded as stated in (9), then

$$\begin{aligned} \|\phi\|^2 &= (\gamma_1 V_{pv})^2 + (-\gamma_2 + \gamma_3)^2 \\ &= \left(\gamma_1^2 V_{pv}^2 + \gamma_2^2 + \gamma_3^2 - 2\gamma_2\gamma_3\right) \end{aligned} \tag{12}$$

Introducing an upper bound $V_{pv} = V_{max}$ corresponding to the maximum PV array voltage, the following inequality is obtained

$$\|\phi\|^2 \leq \underbrace{\left(\gamma_1^2 V_{max}^2 + \gamma_2^2 + \gamma_3^2 - 2\gamma_2\gamma_3\right)}_{\eta_0} \tag{13}$$

The considered output's external disturbance is assumed to be bounded by a constant d_0 as

$$\|w\|^2 \leq d_0 \tag{14}$$

Note that (13) and (14) are not quasi-Lipschitz bounded but Lipschitz bounded instead. Hence, the considered PV system with parametric uncertainty fulfills the required condition for AEM.

4. Design of Luenberger Robust Observer Based on AEM

In this section, the details related to the design of the robust Luenberger observer are presented to obtain a current estimation that allows the PV system to operate in a sensorless way.

Consider the boost based PV system (11) with output y

$$\begin{aligned} \dot{x} &= Ax + g(x)u + D\phi \\ y &= Cx + Ew \end{aligned} \tag{15}$$

where C is the output matrix, D and E are matrix that maps the system uncertainties ϕ and output disturbances w.

The Luenberger observer structure has the following form

$$\dot{\hat{x}} = A\hat{x} + g(x)u + L(y - C\hat{x}) \tag{16}$$

The estimation error is defined as

$$e = x - \hat{x} \tag{17}$$

and its derivative is

$$\begin{aligned} \dot{e} &= \dot{x} - \dot{\hat{x}} \\ &= (A - LC)e + D\phi - LEw \end{aligned} \tag{18}$$

A new extended system z is introduced, which is formed by the estimated state and the estimation error, and its dynamics are as follows

$$\dot{z} = \bar{A}z + F\bar{w} \tag{19}$$

where

$$\bar{A} = \begin{bmatrix} A & LC \\ 0 & A - LC \end{bmatrix}, \quad F = \begin{bmatrix} 0 & LE \\ D & -LE \end{bmatrix}$$
$$z = \begin{bmatrix} \hat{x} & e \end{bmatrix}^T, \quad \bar{w} = \begin{bmatrix} \phi & w \end{bmatrix}^T$$

Introducing a quadratic storage function for the extended system as

$$V(z) = z^T P z, \quad P = \begin{bmatrix} P_1^{-1} & 0 \\ 0 & P_2 \end{bmatrix} \tag{20}$$

To analyze the stability of system it is required to compute the derivative of (20) which has the form

$$\begin{aligned} \dot{V}(z) =& z^T(\bar{A}^T P^{-1} + P^{-1}\bar{A})z + \bar{w}^T F^T P^{-1} z \\ &+ z^T P^{-1} F \bar{w} \end{aligned} \tag{21}$$

and rewriting (21) in a matrix format

$$\dot{V}(z) = \begin{bmatrix} z \\ \bar{w} \end{bmatrix}^T \begin{bmatrix} \bar{A}^T P^{-1} + P^{-1}\bar{A} & P^{-1}F \\ F^T P^{-1} & 0 \end{bmatrix} \begin{bmatrix} z \\ \bar{w} \end{bmatrix} \tag{22}$$

To include the terms related to system uncertainties, these are added and subtracted in the following way

$$\begin{aligned} \dot{V}(z) = \begin{bmatrix} z \\ \phi \\ w \end{bmatrix}^T & \overbrace{\begin{bmatrix} M_{11} & P^{-1}F \\ F^T P^{-1} & \begin{bmatrix} -\tau_1 & 0 \\ 0 & -\tau_2 \end{bmatrix} \end{bmatrix}}^{M} \begin{bmatrix} z \\ \phi \\ w \end{bmatrix} \\ & - \alpha V(z) + \tau_1 \|\phi\|^2 + \tau_2 \|w\|^2 \end{aligned} \tag{23}$$

where

$$M_{11} = \bar{A}^T P^{-1} + P^{-1}\bar{A} + \alpha P^{-1}$$

Substituting (13) and (14)

$$\dot{V}(z) \leq \begin{bmatrix} z \\ \phi \\ w \end{bmatrix}^T M \begin{bmatrix} z \\ \phi \\ w \end{bmatrix} - \alpha V(z) + \tau_1 \eta_0 + \tau_2 d_0 \tag{24}$$

Expanding matrix M a new representation in terms of matrix $\bar{M}$ is obtained as

$$\begin{aligned} \dot{V}(z) \leq \begin{bmatrix} \hat{x} \\ e \\ \phi \\ w \end{bmatrix}^T & \overbrace{\begin{bmatrix} \bar{M}_{11} & \bar{M}_{12} & 0_{n\times m} & \bar{M}_{14} \\ \bar{M}_{12}^T & \bar{M}_{22} & \bar{M}_{23} & \bar{M}_{24} \\ 0_{m\times n} & \bar{M}_{23}^T & -\tau_1 & 0_{m\times n} \\ \bar{M}_{14}^T & \bar{M}_{24}^T & 0_{n\times m} & -\tau_2 \end{bmatrix}}^{\bar{M}} \begin{bmatrix} \hat{x} \\ e \\ \phi \\ w \end{bmatrix} \\ & - \alpha V(z) + \tau_1 \eta_0 + \tau_2 d_0 \end{aligned} \tag{25}$$

with

$$\bar{M}_{11} = A^T P_1^{-1} + P_1^{-1} A + \alpha P_1^{-1} \ , \ \bar{M}_{12} = P_1^{-1} LC$$
$$\bar{M}_{22} = A^T P_2 + P_2 A - C^T L^T P_2 + \alpha P_2 - P_2 LC$$
$$\bar{M}_{23} = P_2 D \ , \ \bar{M}_{14} = P_1^{-1} LE \ , \ \bar{M}_{24} = -P_2 LE$$

A non-singular transformation is applied to matrix $\bar{M}$ in order to eliminate the inverse matrix operations. Such transformation has the following form

$$M_1 = T_1 \bar{M} T_1^T \ , \ T_1 = diag[P_1, I_{n\times n}, I_{m\times m}, I_{m\times m}] \tag{26}$$

$$M_1 = \begin{bmatrix} P_1 A^T + A P_1 + \alpha P_1 & LC & 0 & LE \\ C^T L^T & \bar{M}_{22} & P_2 D & -P_2 LE \\ 0 & D^T P_2 & -\tau_1 & 0 \\ E^T L^T & -E^T L^T P_2 & 0 & -\tau_2 \end{bmatrix} \tag{27}$$

Finally, inequality (25) results in

$$\dot{V}(z) \leq \begin{bmatrix} \hat{x} \\ e \\ \phi \\ w \end{bmatrix}^T M_1 \begin{bmatrix} \hat{x} \\ e \\ \phi \\ w \end{bmatrix} - \alpha V(z) + \tau_1 \eta_0 + \tau_2 d_0 \tag{28}$$

if some matrices P_1, P_2 and L that satisfies $M_1 < 0$ exist, then the following holds

$$\dot{V}(z) \leq -\alpha V(z) + \beta \tag{29}$$

and $\mathcal{E}(P)$ is the ellipsoid that guarantees convergence and boundedness of the estimation error trajectories.

In order to obtain the values of P_1, P_2 and L that satisfies the condition $M_1 < 0$ an optimization problem is defined. This procedure is related to minimization of the ellipsoid size which is achieved by minimizing the trace of matrix P under the constraints τ_1, τ_2, α stated in (27). Such an optimization problem is defined as

$$\min_{P,L,\tau_1,\tau_2,\alpha} \quad trace(P) \tag{30}$$

$$\begin{aligned} subject\ to \quad & M_1 < 0 \\ & \alpha > \tau_1 \eta_0 + \tau_2 d_0 \end{aligned}$$

Observe that (27) is a BMI due to multiplication of design variables (this is, αP). To solve optimization problems subject to bilinear constraints arising in the AEM based design, an iterative procedure based on LMI has been applied in [25,26]. Using this iterative procedure, the corresponding optimization problem (30) can be solved using an LMI solver such as SEDUMI without the need of specialized BMI solvers.

Incremental Conductance MPPT Algorithm

The incremental conductance algorithm is based on detection of the slope of the P-V curve, and the MPP is tracked by searching the peak of the P-V curve. As the name implies, this algorithm makes use of the incremental conductance dI/dV and the instantaneous conductance I/V to perform MPPT. The operating point location of the PV module in the P-V curve can be determined based on the relationship between conductance values as follows

$$\frac{dI}{dV} = -\frac{I}{V} \tag{31}$$

$$\frac{dI}{dV} > -\frac{I}{V} \tag{32}$$

$$\frac{dI}{dV} < -\frac{I}{V} \tag{33}$$

where (31) corresponds to PV module operating at the MPP, while (32) and (33) indicate the PV module operation is located at the left and right side of the MPP in the P-V curve, respectively.

Equations (31)–(33) are obtained from the fact that slope of the P-V curve at MPP is equal to zero, that is

$$\frac{dP}{dV} = 0 \tag{34}$$

and since $P = VI$, (34) can be rewritten with the following form

$$I + V\frac{dI}{dV} = 0 \tag{35}$$

The conventional INC algorithm achieves the MPP detection using (35), and the PV module voltage and current are measured by the MPPT controller. If (32) is fulfilled, the duty cycle of the DC-DC converter is decreased while if (33) is satisfied the duty cycle is increased. On the other hand, duty cycle keep the same value for the case where (35) is satisfied [33]. The overall operation of INC algorithm is depicted in Figure 3.

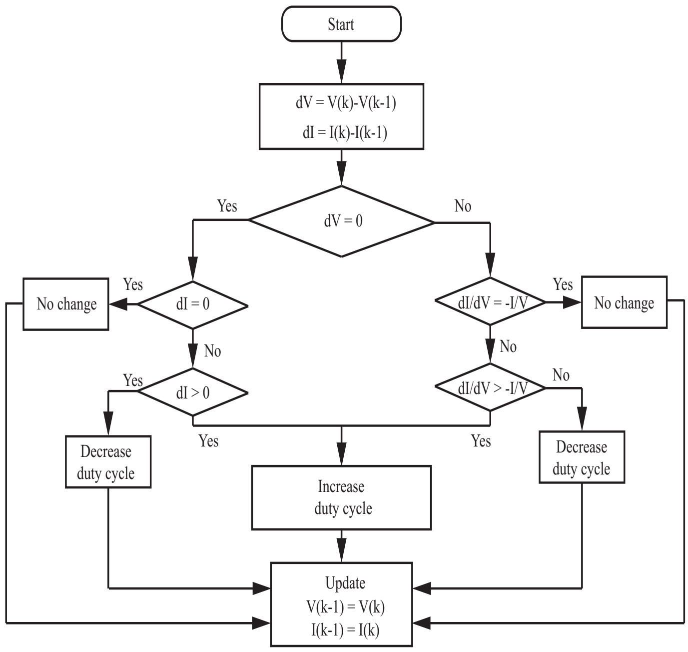

Figure 3. Flow chart of INC algorithm.

5. Results

To verify the performance of the designed robust observer, simulations are developed in Matlab/Simulink environment using the toolbox Simscape/Power Systems which contains specialized functions to model power converter components and PV systems. The parameters of the selected PV module used in simulation are presented in Table 1 and the ones corresponding to boost converter are shown in Table 2.

Table 1. Parameters of PV panel 1Soltech 1STH-240-WH.

Parameter	Description	Value
P_{max}	Maximum power	239.68 W
V_{oc}	Open circuit voltage	37.1 V
I_{sc}	Short-circuit current	8.58 A
V_{mpp}	Voltage at MPP	29.7 V
I_{mpp}	Current at MPP	8.07 A

Table 2. Boost converter's parameters.

Parameter	Description	Value
L_b	Inductor	0.988 mH
C_b	Output capacitor	1880 µF
R	Load resistance	5 Ω

The simulation is based on a small scale system which is composed only by 1 PV panel, its corresponding P-V and I-V curves showing the maximum power point are illustrated in Figure 4 and Figure 5, respectively.

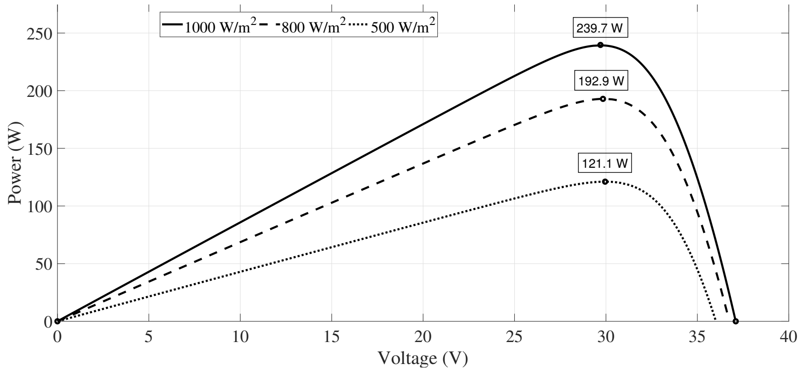

Figure 4. P-V curve for PV module 1Soltech 1STH-240-WH.

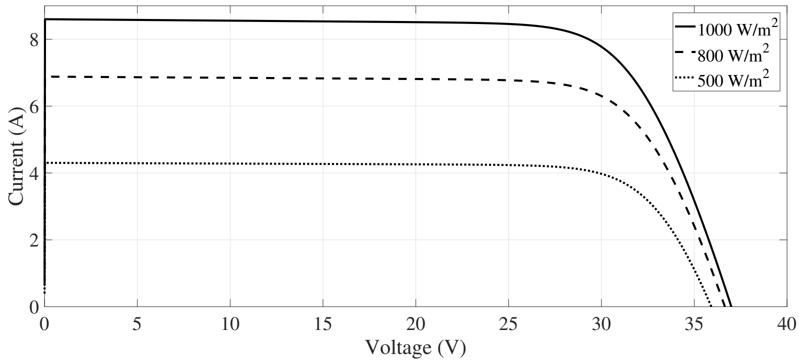

Figure 5. I-V curve for PV module 1Soltech 1STH-240-WH.

The proposed observer gain matrix L and ellipsoid size matrix P obtained by solving the optimization problem (30) with a parameter uncertainty equal to 10% of the nominal component value (for R,L_b,C_b) are

$$L = \begin{bmatrix} 1.8522 \\ 0.1190 \end{bmatrix} \times 10^4 \quad P_1 = \begin{bmatrix} 1.1489 & 0.1031 \\ 0.1031 & 0.6071 \end{bmatrix} \times 10^5,$$

$$P_2 = \begin{bmatrix} 4.4802 & -5.0986 \\ -5.0986 & 165 \end{bmatrix} \times 10^{-4},$$

$$\alpha = 31.6248 \ , \ \tau_1 = 1.5180 \times 10^{-4} \ , \ \tau_2 = 131.7717 \ .$$

The first simulation scenario is for two fixed values of solar irradiation at 800 W/m^2 and 1000 W/m^2 as shown in Figure 6.

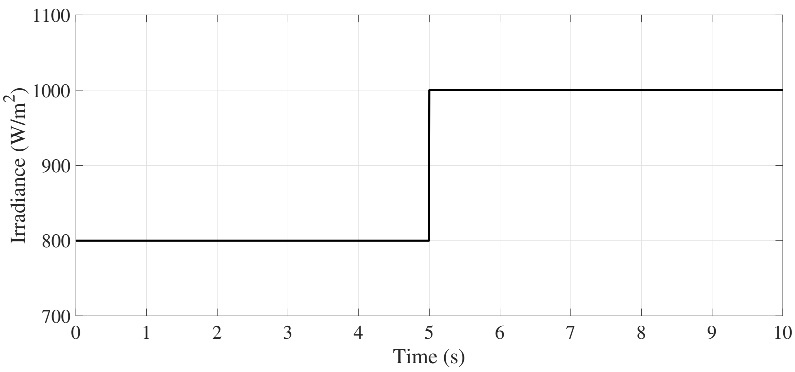

Figure 6. Irradiation profile for fixed values.

The PV current is depicted in Figure 7 where x_1 and x_{1e} stands for the ideal measured state and estimated state, respectively. The estimated current follows the actual current with high speed and an acceptable precision for both irradiation levels but decreases for higher current values. A similar situation is observed in Figure 8 for the output voltage x_2.

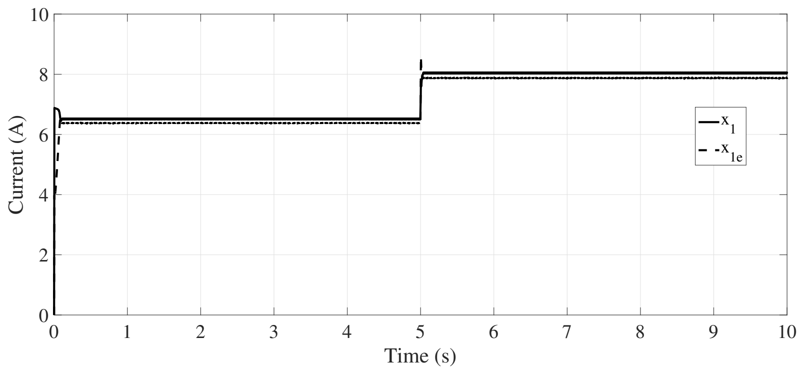

Figure 7. PV current.

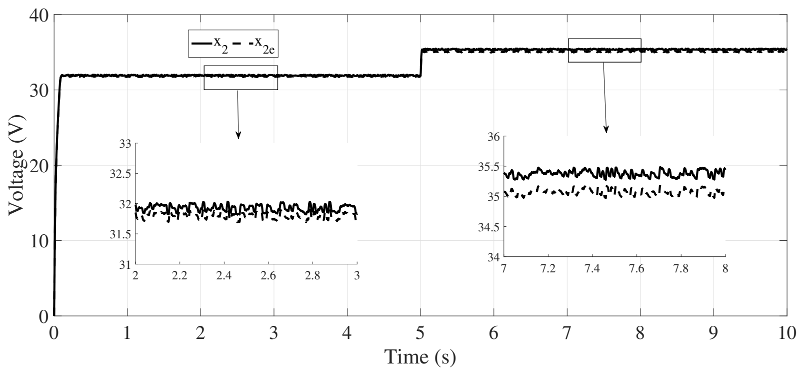

Figure 8. Output voltage.

The error signal for both states is illustrated in Figure 9 where is observed an error value lower than 2% for both irradiation conditions which verifies an efficient estimation under the proposed parameter variation. This result indicates that the estimated current can be a good alternative for current based MPPT techniques as Incremental Conductance algorithm, allowing a current sensorless operation.

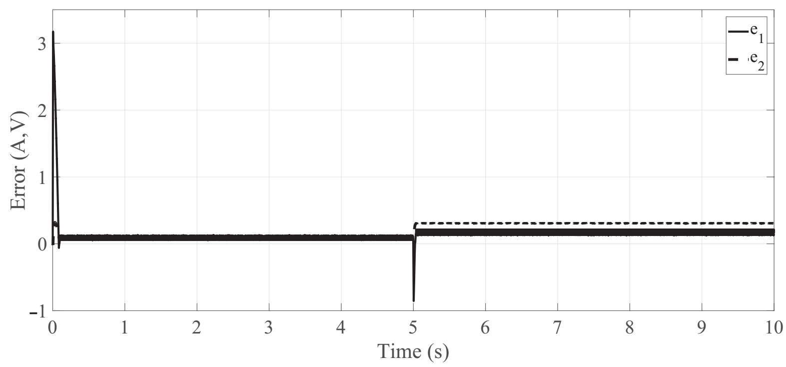

Figure 9. The error of estimation.

The second simulation corresponds to the application of the designed observer to achieve MPPT using a conventional current based technique as the INC algorithm. The INC algorithm depends on measures of PV voltage and current, then the current sensor is substituted for the designed robust observer. An irradiation profile based on the European standard EN50530 is constructed which contains oscillations of different period between two values located approximately in the middle section of PV module operating range. This irradiation profile is depicted in Figure 10.

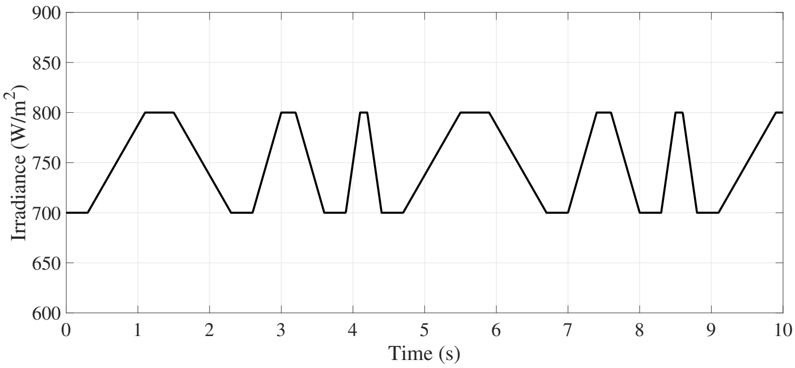

Figure 10. Irradiation profile based on EN50530 standard.

The estimation of PV current and output voltage for the MPPT test is shown in Figure 11 and Figure 12, respectively. A good tracking of the actual values is observed for both states, but some small oscillations are present due to the constant solar irradiation changes introduced as input for the PV system in the test profile.

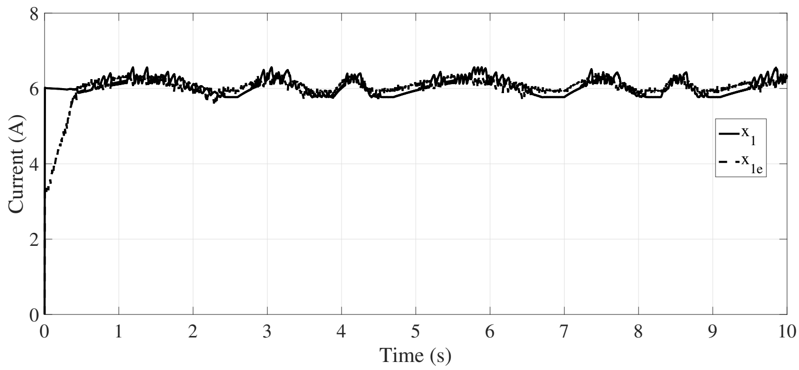

Figure 11. PV current for MPPT test.

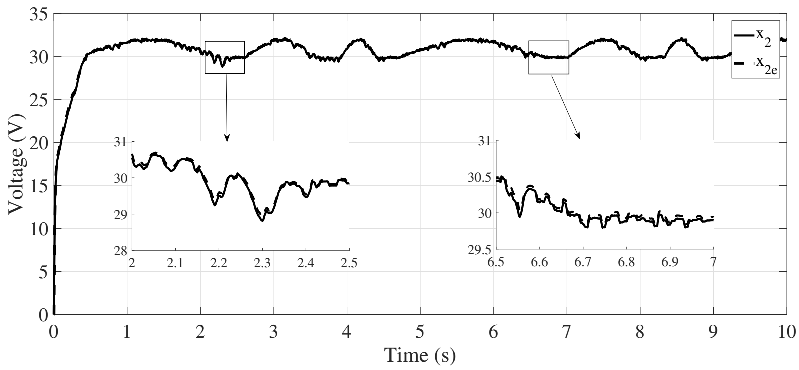

Figure 12. Output voltage for MPPT test.

In Figure 13, the estimation error for the MPPT test is presented. It can be seen that the estimation error has a low value for both states which confirms an appropriate performance of the designed observer for a changing irradiation situation. However, the estimated current shows some oscillations that generate error peak values of almost 0.5, which will deteriorate the MPPT performance affecting the generated power.

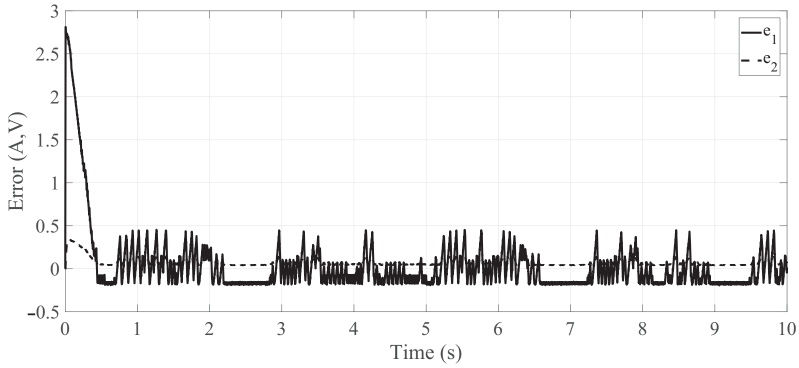

Figure 13. Error signals for MPPT test.

This MPPT performance deterioration can be observed in the PV system's generated power behavior which is illustrated in Figure 14. The generated power using the proposed current sensorless scheme has a similar behavior than the conventional measurement based scheme, which indicates the feasibility of the proposal. Nevertheless, despite the good estimation and operation of the sensorless scheme, there are power losses caused by the current estimation error. Such losses can be reduced by improving the observer's parameters which leads to a better current estimation. Figure 15 shows the power error between the conventional INC scheme and the sensorless proposal, the power losses caused by the estimation error are evident but also small. The average value for this error is 1.15% in the range t = 0.5–10 s. Hence, this power losses are small enough to be a good trade-off for eliminating the cost associated with a current sensor, mainly when working with small scale domestic PV systems.

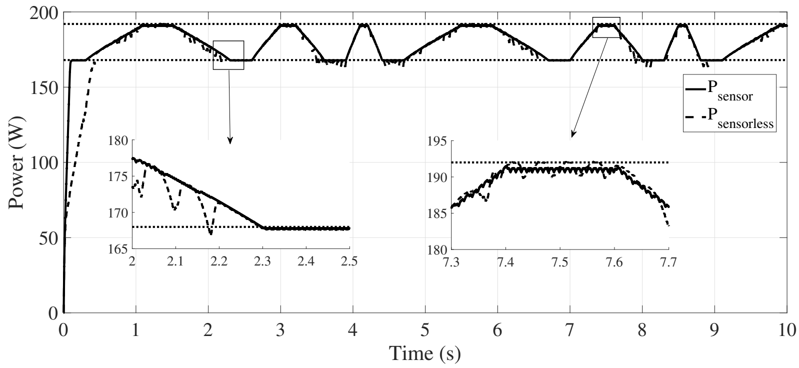

Figure 14. Generated power.

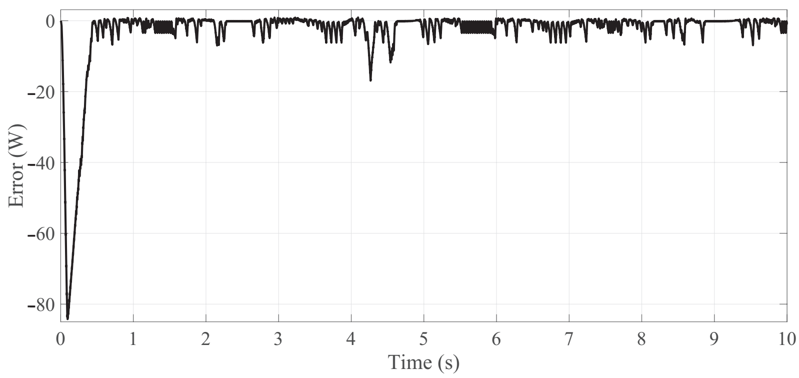

Figure 15. Power error between measured and sensorless based INC algorithm.

6. Conclusions

The proposed robust observer based on Attractive Ellipsoid Method shows a good performance under parameter uncertainty in the boost power converter and noise in the output signal. The computation of the observer gains is done by means of solving an LMI optimization problem derived from the AEM, which guarantees the convergence of the estimation error under the considered uncertainties and external disturbances. The estimation error of the designed observer is low and has enough convergence speed to track the real state values, which allows the utilization of the estimated current for MPPT operation with the drawback of be limited to implementation of current based MPPT techniques. We demonstrated the appropriate operation of a conventional Incremental Conductance algorithm for MPPT in the proposed sensorless form under a test based on European standard EN50530 with small power losses due to current estimation error. Nevertheless, such power loss represents a good trade-off for the elimination of current sensor's cost mainly when operating small scale domestic PV systems. Although the observer is robust against parameter uncertainties, the variable nature of PV systems operating conditions as temperature, humidity or solar irradiance level may affect its performance and should be considered in the design stage. The effect of such conditions in the PV system performance and the experimental stage of the proposed scheme are considered as future research works.

Author Contributions: Conceptualization, D.C.-V.; Investigation, J.L.R.-L.; Resources, J.L.R.-L.; Supervision, H.A.; Writing—original draft, D.C.-V.; Writing—review & editing, H.A. All authors have read and agreed to the published version of the manuscript.

Funding: This research received no external funding.

Data Availability Statement: No new data were created or analyzed in this study. Data sharing is not applicable to this article.

Conflicts of Interest: The authors declare no conflict of interest.

References

1. Kollimalla, S.K.; Mishra, M.K. Variable perturbation size adaptive P&O MPPT algorithm for sudden changes in irradiance. *IEEE Trans. Sustain. Energy* **2014**, *5*, 718–728.
2. Loukriz, A.; Haddadi, M.; Messalti, S. Simulation and experimental design of a new advanced variable step size Incremental Conductance MPPT algorithm for PV systems. *ISA Trans.* **2016**, *62*, 30–38. [CrossRef] [PubMed]
3. Messalti, S.; Harrag, A.; Loukriz, A. A new variable step size neural networks MPPT controller: Review, simulation and hardware implementation. *Renew. Sustain. Energy Rev.* **2017**, *68*, 221–233. [CrossRef]
4. Kulaksız, A.A.; Akkaya, R. A genetic algorithm optimized ANN-based MPPT algorithm for a stand-alone PV system with induction motor drive. *Sol. Energy* **2012**, *86*, 2366–2375. [CrossRef]
5. Algazar, M.M.; El-Halim, H.A.; Salem, M.E.E.K. Maximum power point tracking using fuzzy logic control. *Int. J. Electr. Power Energy Syst.* **2012**, *39*, 21–28. [CrossRef]
6. Life Energy Motion (LEM). Datasheet: Current Transducer LTSR 6-NP. 2017. Available online: www.lem.com.
7. Ziegler, S.; Woodward, R.C.; Iu, H.H.C.; Borle, L.J. Current sensing techniques: A review. *IEEE Sens. J.* **2009**, *9*, 354–376. [CrossRef]
8. Chen, Y.; Huang, Q.; Khawaja, A.H. An interference-rejection strategy for measurement of small current under strong interference with magnetic sensor array. *IEEE Sens. J.* **2018**, *19*, 692–700. [CrossRef]
9. Honeywell. Hall Effect Sensing and Application. Available online: https://sensing.honeywell.com/honeywell-sensing-sensors-magnetoresistive-hall-effect-applications-005715-2-en2.pdf (accessed on 15 December 2021).
10. Itzke, A.; Weiss, R.; Weigel, R. Influence of the conductor position on a circular array of Hall sensors for current measurement. *IEEE Trans. Ind. Electron.* **2018**, *66*, 580–585. [CrossRef]
11. Min, R.; Tong, Q.; Zhang, Q.; Zou, X.; Yu, K.; Liu, Z. Digital sensorless current mode control based on charge balance principle and dual current error compensation for DC–DC converters in DCM. *IEEE Trans. Ind. Electron.* **2015**, *63*, 155–166. [CrossRef]
12. Yu, B.; Abo-Khalil, A.G. Current estimation based maximum power point tracker of grid connected PV system. In Proceedings of the 2013 IEEE 10th International Conference on Power Electronics and Drive Systems (PEDS), Kitakyushu, Japan, 22–25 April 2013; pp. 948–952.
13. Wang, Y.; Liu, Y.; Wang, C.; Li, Z.; Sheng, X.; Lee, H.G.; Chang, N.; Yang, H. Storage-less and converter-less photovoltaic energy harvesting with maximum power point tracking for internet of things. *IEEE Trans. Comput.-Aided Des. Integr. Circuits Syst.* **2015**, *35*, 173–186. [CrossRef]
14. Ahmed, M.; Abdelrahem, M.; Kennel, R.; Hackl, C.M. A robust maximum power point tracking based model predictive control and extended Kalman filter for PV systems. In Proceedings of the 2020 International Symposium on Power Electronics, Electrical Drives, Automation and Motion (SPEEDAM), Sorrento, Italy, 24–26 June 2020; pp. 514–519.

15. Mattavelli, P. Digital control of DC-DC boost converters with inductor current estimation. In Proceedings of the Nineteenth Annual IEEE Applied Power Electronics Conference and Exposition, 2004. APEC'04, Anaheim, CA, USA, 22–26 February 2004; Volume 1, pp. 74–80.
16. Zhang, Y.; Zhao, Z.; Lu, T.; Yuan, L.; Xu, W.; Zhu, J. A comparative study of Luenberger observer, sliding mode observer and extended Kalman filter for sensorless vector control of induction motor drives. In Proceedings of the 2009 IEEE Energy Conversion Congress and Exposition, San Jose, CA, USA, 20–24 September 2009; pp. 2466–2473.
17. Kandepu, R.; Foss, B.; Imsland, L. Applying the unscented Kalman filter for nonlinear state estimation. *J. Process Control* **2008**, *18*, 753–768. [CrossRef]
18. Metry, M.; Balog, R.S. An Adaptive Model Predictive Controller for Current Sensorless MPPT in PV Systems. *IEEE Open J. Power Electron.* **2020**, *1*, 445–455. [CrossRef]
19. Valenciaga, F.; Inthamoussou, F.A. A novel PV-MPPT method based on a second order sliding mode gradient observer. *Energy Convers. Manag.* **2018**, *176*, 422–430. [CrossRef]
20. Pati, A.K.; Sahoo, N.C. Super-Twisting Sliding Mode Observer for Grid-Connected Differential Boost Inverter based PV System. In Proceedings of the IECON 2019-45th Annual Conference of the IEEE Industrial Electronics Society, Lisbon, Portugal, 14–17 October 2019; Volume 1, pp. 4025–4030.
21. Stitou, M.; El Fadili, A.; Chaoui, F.Z.; Giri, F. Output feedback control of sensorless photovoltaic systems, with maximum power point tracking. *Control Eng. Pract.* **2019**, *84*, 1–12. [CrossRef]
22. Esfandiari, F.; Khalil, H.K. Output feedback stabilization of fully linearizable systems. *Int. J. Control* **1992**, *56*, 1007–1037. [CrossRef]
23. Das, D.; Madichetty, S.; Singh, B.; Mishra, S. Luenberger observer based current estimated boost converter for PV maximum power extraction—A current sensorless approach. *IEEE J. Photovolt.* **2018**, *9*, 278–286. [CrossRef]
24. Poznyak, A.; Polyakov, A.; Azhmyakov, V. *Attractive Ellipsoids in Robust Control*; Springer: Cham, Switzerland, 2014.
25. Alazki, H.; Hernández, E.; Ibarra, J.M.; Poznyak, A. Attractive ellipsoid method controller under noised measurements for SLAM. *Int. J. Control Autom. Syst.* **2017**, *15*, 2764–2775. [CrossRef]
26. Alazki, H.; Poznyak, A.S. A class of robust bounded controllers tracking a nonlinear discrete-time stochastic system: Attractive ellipsoid technique application. *J. Frankl. Inst.* **2013**, *350*, 1008–1029. [CrossRef]
27. Medina-García, J.; Martín, A.D.; Cano, J.M.; Gómez-Galán, J.A.; Hermoso, A. Efficient wireless monitoring and control of a grid-connected photovoltaic system. *Appl. Sci.* **2021**, *11*, 2287. [CrossRef]
28. Samano-Ortega, V.; Padilla-Medina, A.; Bravo-Sanchez, M.; Rodriguez-Segura, E.; Jimenez-Garibay, A.; Martinez-Nolasco, J. Hardware in the Loop Platform for Testing Photovoltaic System Control. *Appl. Sci.* **2020**, *10*, 8690. [CrossRef]
29. Leyva, R.; Cid-Pastor, A.; Alonso, C.; Queinnec, I.; Tarbouriech, S.; Martinez-Salamero, L. Passivity-based integral control of a boost converter for large-signal stability. *IEE Proc.-Control. Theory Appl.* **2006**, *153*, 139–146. [CrossRef]
30. Olalla, C.; Leyva, R.; El Aroudi, A.; Queinnec, I. Robust LQR control for PWM converters: An LMI approach. *IEEE Trans. Ind. Electron.* **2009**, *56*, 2548–2558. [CrossRef]
31. Kassakian, J.G.; Schlecht, M.F.; Verghese, G.C. *Principles of Power Electronics*; Addison Wesley: Boston, MA, USA, 1991.
32. Krein, P.T.; Bentsman, J.; Bass, R.; Lesieutre, M.B.L. On the use of averaging for the analysis of power electronic systems. *IEEE Trans. Power Electron.* **1990**, *5*, 182–190. [CrossRef]
33. Mei, Q.; Shan, M.; Liu, L.; Guerrero, J.M. A novel improved variable step-size incremental-resistance MPPT method for PV systems. *IEEE Trans. Ind. Electron.* **2010**, *58*, 2427–2434. [CrossRef]